J. Construct. Steel Research 24 (1993) 105–119

Behaviour of Thin-Walled Steel Frame Joints

I. Vayas

National Technical University of Athens, Greece

&

D. Briassoulis

Agricultural University of Athens, Greece

(Received 10 October 1991; revised version received 10 January 1992; accepted 3 March 1992)

ABSTRACT

Welded thin-walled plate girders play an increasingly important role in steel structures. The provisions of modern codes with regard to design are restricted to the span region between supports. The design of the joint panel is still governed by the buckling load, thus making the application of costly stiffeners necessary. Experimental investigations on such joints have shown that their strength is well above this load, due to the development of a tension field action. To ensure an effective design, it is necessary to make allowance for the postbuckling reserve of strength and to identify possible collapse mechanisms.

The present paper provides a method for calculating the carrying capacity and the deformation characteristics of the joints. Static and kinematic limit state models are presented which allow the ultimate strength to be determined from closed formulae. The predicted values are in reasonable agreement with experimental results.

INTRODUCTION

Welded thin-walled plate girders play an increasingly more important role in steel structures. The main reasons for this development are (a) the introduction of modern fabrication methods regarding the welding of plates, (b) the fact that the geometry of a plate girder with respect to the

J. Construct. Steel Research 0143-974X/93/$06·00

thickness of the flanges and the web can be selected to fit best to the strain conditions of a structural element and (c) the results of intensive experimental and theoretical research enabled the design of girders for loads higher than the buckling loads.

The provisions of all modern Codes regarding the design of thin-walled plate girders of class 4 webs are, however, restricted to the span region between supports. The design of the joint panel is still governed by the buckling load, thus making the application of costly diagonal stiffeners or backing plates necessary. In order to provide information on the postcritical behaviour of such joints, tests have been performed at the Institute for Steel Structures in Braunschweig, Germany, which were reported by Scheer *et al.*[1] Those tests supplied evidence that the joint panels exhibit a significant reserve strength beyond buckling. A design method for the joint, included in that report, is based on the tension field method for girders that are adequately adapted to the loading and boundary conditions of a joint.

The behaviour of thin-walled joints can be directly related to the corresponding behaviour of joints of normal thickness, extensively investigated for the postyielding range at Berkeley, USA.[2,3] The reason for these investigations was to allow plastification of the web panel in order to participate in the dissipation of the seismic input energy.

The tests of Braunschweig showed that the behaviour of the joint in the postbuckling range is largely controlled by the properties of the elements surrounding the panel. The tests at Berkeley indicated the same effect for the behaviour of the web panel in the postyielding range.

Another characteristic that was investigated experimentally concerned the deformations of the joints. When the joints are designed beyond the linear (postbuckling or postyielding) range, it is important to include the deformations in the overall analysis of the frame, since its lateral sway may become critical due to P–Δ effects. Such information is provided only for joints with web panels of normal thickness.[2,4] For thin-walled webs, where these deformations are even more important, no information is available at the present.

This paper deals with the postbuckling behaviour of joints with thin-walled web panels. Two limit state models, one 'static' and one 'kinematic', are presented which lead to closed formulae for the determination of the ultimate limit strength of the joint. The results obtained by the proposed models as well as those of other available models are compared against existing experimental results, in order to investigate whether the methods used for thick webs also apply to thin ones. In addition, the proposed models supply information on the deformation characteristics of the joints.

This enables the inclusion of joint deformations in the overall analysis of the frames, e.g. according to the joint model proposed by Ermopoulos & Vayas.[5]

The present models refer to square joints for which experimental results exist. They can, however, easily be extended to rectangular joints.

A STATIC MODEL FOR THE FAILURE MECHANISM

The limit state model refers to a square joint as shown in Fig. 1. The joint is provided with horizontal stiffeners in order to avoid crippling the web panel due to the concentrated flange forces. The mechanism of failure may be adequately described from the Braunschweig test.[1] In those experiments all joints tested appeared to experience failure associated with the formation of plastic hinges, leading to the mechanism described schematically in Fig. 2. The failure mechanism experiences the development of a

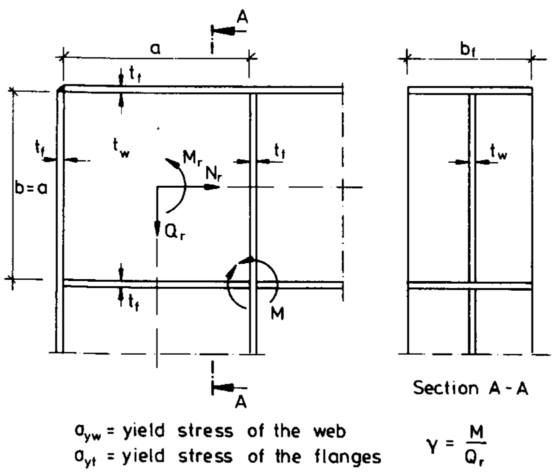

Fig. 1. Geometry of the joint, notation.

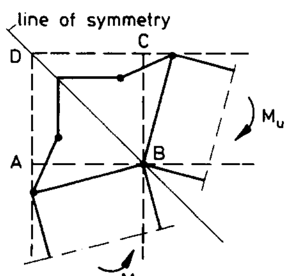

Fig. 2. A failure mechanism for the joint.

strong shear tension field directed along the diagonal AC. The tension field may be assumed to extend between the plastic hinges formed on the sides of the external flanges AD and DC and a portion of the sides of the internal flanges. The mechanism is considered to be symmetric with respect to the diagonal BD of the joint, which implies symmetric loading conditions for the joint ($N_r = Q_r$ in Fig. 1). This assumption may be kept for the general case of non-symmetric loading, since the behaviour of the joints is due to the usual geometric characteristics of the overall frames where beams with thin webs are applied (long spans, small shear ratios), primarily governed by moments and not by axial or shear forces. This observation has been confirmed by the test results.

Using the properties of symmetry, a 'static' model is constructed in accordance with the failure mechanism of Fig. 1, as shown in Fig. 3. The tension field is considered to develop the full yield stresses σ_{yw} of the panel zone material, without accounting for any reduction of the shear stress τ_{cr} that develops prior to shear buckling. The effects of this assumption do compensate to some extent for the neglection of strain hardening, which is expected to develop at large rotations in the vicinity of the ultimate moment. Additionally, τ_{cr} is difficult to determine accurately, given the uncertainty in defining the boundary conditions.

The analysis of the ultimate moment of the joint at failure is based on the statics of the symmetric half of the joint after all plastic hinges have been formed. The tension field is simulated by its tension force resultants T_1 and T_2 on the two adjacent sides of point C. All plastic hinges are considered to develop equal plastic moments M_p, given by

$$M_p = \sigma_{yf} \frac{b_f t_f^2}{4} \tag{1}$$

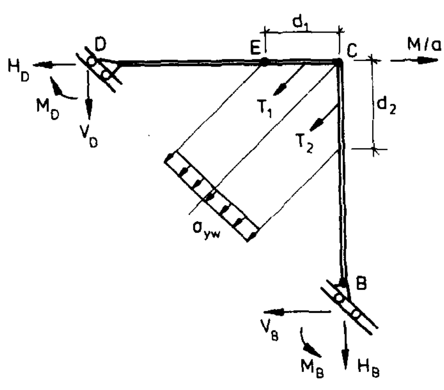

Fig. 3. The static model.

where the effect of the axial forces on M_p is ignored. Then, applying the equation of equilibrium described by the statics of the system in the elements DE, EC and BC successively and solving the resulting simultaneous equations, one obtains for the ultimate moment M_u of the joint:

$$M_u = [Ad_1 + B\frac{1}{d_1} + C] \tag{2}$$

where

$$A = \sigma_{yw} t_w \frac{\alpha}{4} \tag{3}$$

$$B = 2\alpha M_f \tag{4}$$

$$C = 2M_p + \sigma_{yw} t_w \frac{d_2}{2}\left(\alpha - \frac{d_2}{2}\right) \tag{5}$$

Differentiating eqn (2) with respect to the unknown distances d_1 and d_2 and equating the corresponding partial differentials to zero to minimize the ultimate moment M_u with respect to d_1 and d_2, one finds the critical distances d_1 and d_2 for which the failure mechanism develops with the least energy. These differentiations yield the following relationships for the distances d_1 and d_2, normalized to the length of the panel:

$$\frac{d_1}{a} = \sqrt{2\left(\frac{\sigma_{yf}}{\sigma_{yw}}\right)\left(\frac{b_f}{a}\right)\left(\frac{t_f}{t_w}\right)\left(\frac{t_f}{a}\right)} \tag{6}$$

$$\frac{d_2}{a} = 1 \tag{7}$$

Substitution of eqns (3)–(7) into eqn (2) yields the following closed formula for the ultimate moment of the joint:

$$M_u = \frac{a^2 t_w \sigma_{yw}}{\sqrt{3}} \frac{\sqrt{3}}{4}\left(1 + \frac{d_1}{a}\right)^2 \tag{8}$$

A KINEMATIC MODEL OF THE FAILURE MECHANISM

From measurements on the test specimens after failure, a second, more accurate (in relation to the geometric properties), failure mechanism may be derived (Fig. 4). The mechanism is constructed by subsequently

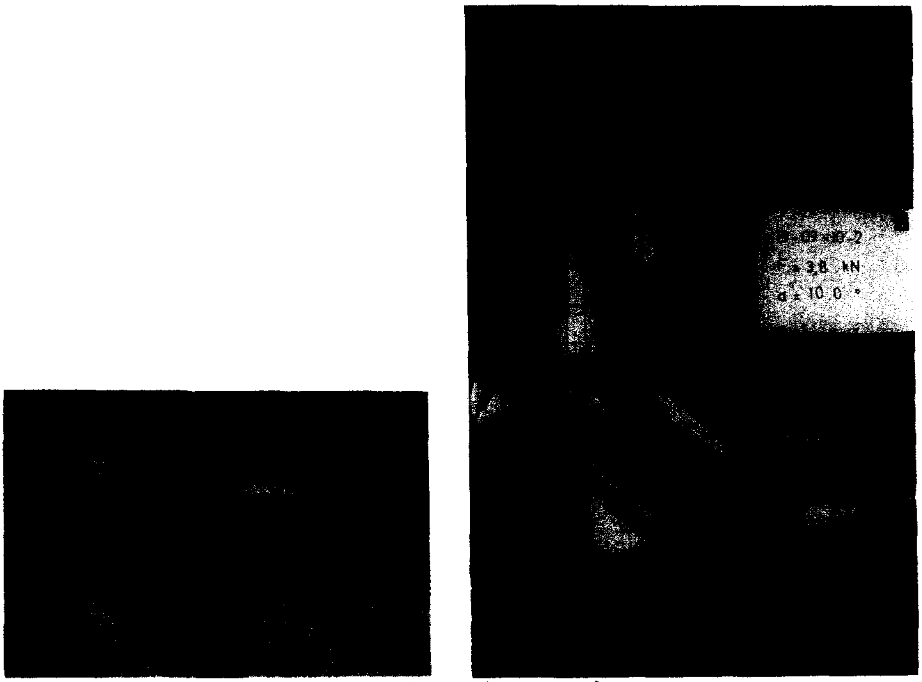

Fig. 4(a) Joints at large rotations;

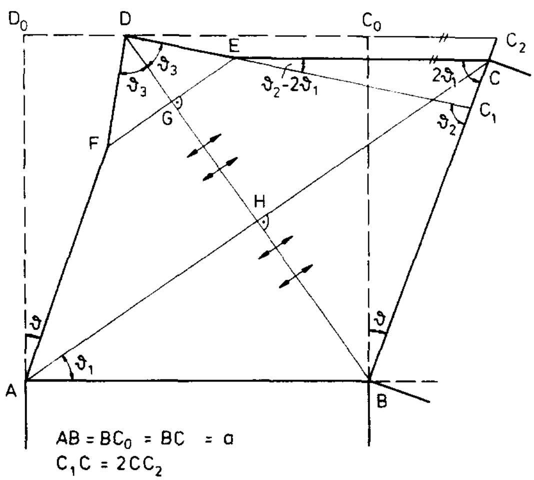

Fig. 4(b) Joint at failure for the kinematic model.

determining, for a given angle of rotation, the points C, C_2, D, E and F according to the geometric relations or as intersections of two straight lines, as indicated in Fig. 4. The failure mechanism experiences the development of six plastic hinges and a tension field directed along the diagonal. All geometric properties of the failure mechanism may be determined as a function of the angle of rotation θ, making use of trigonometric relations. The angles are given by the expressions:

$$\theta_1 = \frac{\pi}{4} - \frac{\theta}{2} \tag{9}$$

$$\tan\theta_2 = \frac{\sin(\theta+\theta_1)}{(3-2/\cos\theta)\cos\theta_1 - \cos(\theta+\theta_1)} \tag{10}$$

$$\theta_3 = \pi - \theta - \theta_1 - \theta_2 \tag{11}$$

The lengths are given by

$$\mathrm{EC}_1 = 2a\left(\frac{1}{\cos\theta} - 1\right)\frac{\sin\theta_2}{\sin(\theta_2 - 2\theta_1)} \tag{12}$$

$$\mathrm{HG} = \mathrm{EC}_1 \sin\theta_1 \tag{13}$$

$$\mathrm{BH} = a\sin\theta_1 \tag{14}$$

and the elongation of the diagonal AC by

$$\delta(\mathrm{AC}) = 2a\cos\theta_1 - a\sqrt{2} \tag{15}$$

The analysis for the ultimate moment of the joint at failure is based on the expression of the work done by the external and internal forces and moments. The internal work is composed of two terms, one representing the work done by the panel zone web equal to

$$U_1^{\mathrm{T}} = \tfrac{1}{2}\mathrm{BG}\,\sigma_{yw} t_w \delta(\mathrm{AC}) \tag{16}$$

and the other representing the work done by the plastic hinges. Assuming that all flanges have equal plastic moments, this work is equal to

$$U_2^{\mathrm{T}} = M_p\left[\theta + \theta + (\theta_2 - 2\theta_1) + \left(2\theta_3 - \frac{\pi}{2}\right) + (\theta_2 - 2\theta_1) + \theta\right] = 4M_p\theta \tag{17}$$

where M_p is given by eqn. (1). The work done by the external forces and moments according to Fig. 1 is equal to

$$W^{T} = -M_{r} \sin\theta + \frac{N_{r}}{2} a \sin\theta + \frac{Q_{r}}{2} a(1-\cos\theta)$$

$$= -M\left[\sin\theta - \frac{a(1-\cos\theta)}{2\gamma}\right] \tag{18}$$

The ultimate limit moment M_u at failure may then be determined by setting equal the internal to the external work:

$$W^{T} = U_{1}^{T} + U_{2}^{T} \tag{19}$$

according to

$$-M_{u}\left[\sin\theta - \frac{a(1-\cos\theta)}{2\gamma}\right]$$

$$= \frac{1}{2}(\mathrm{EC}_{1} + a)\sin\theta_{1}\sigma_{yw}t_{w}(2a\cos\theta_{1} - a\sqrt{2}) + 4M_{p}\theta \tag{20}$$

The value of M_u is expressed according to eqn (20) in terms of the angle of ration θ. This angle is, however, unknown and will be eliminated. This may be done by assuming its values to be small, so that eqn (20) then becomes

$$-M_{u}\theta = \tfrac{3}{8}a^{2}\sigma_{yw}t_{w}\theta + 4M_{p}\theta \tag{21}$$

The ultimate limit moment may then be determined by substituting eqn (1) in eqn (21), which yields

$$M_{u} = -\frac{\sigma_{yw}t_{w}a^{2}}{\sqrt{3}}\left(0{\cdot}65 + \frac{3{\cdot}45t_{f}^{2}}{at_{w}}\frac{\sigma_{yf}}{\sigma_{yw}}\frac{b_{f}}{2a}\right) \tag{22}$$

The first term in eqn (22) represents the carrying capacity of the panel zone web, whereas the second one represents the carrying capacity of the surrounding frame. It must be noted that eqns (8) and (22) give the ultimate limit moment at the internal corner i of the joint, as shown in Fig. 1.

COMPARISON BETWEEN EXPERIMENTAL AND OTHER ANALYTICAL RESULTS

As mentioned before, it is known that even for thick web panels the surrounding frame, composed of the column or beam flanges and any stiffeners, contributes to the carrying capacity beyond the yield moment of the web:

$$M_y = a^2 t_w \sigma_{yw}/\sqrt{3} \tag{23}$$

Relative formulae are provided for stiffened joints by the Californian Earthquake Regulations[6] and the Swiss Code for Steel Structures[7] and for unstiffened joints by Tschemmernegg *et al.*[4] These formulae, written with the notation of Fig. 1 and expressed in terms of the ultimate moment, are given by

$$M_u = -\frac{a^2 t_w \sigma_{yw}}{\sqrt{3}}\left(1 + \frac{1{\cdot}43 t_f^2}{a t_w}\frac{b_f}{2a}\right) \tag{24}$$

according to Ref. 6,

$$M_u = -\frac{a^2 t_w \sigma_{yw}}{\sqrt{3}}\left(0{\cdot}7 + \frac{2{\cdot}6 t_f^2}{a t_w}\frac{b_f}{2a}\right) \tag{25}$$

according to Ref. 7 and

$$M_u = -\frac{a^2 t_w \sigma_{yw}}{\sqrt{3}}\left[0{\cdot}66\left(1 + \frac{a}{240 t_f}\right) + \frac{5{\cdot}25 t_f^2}{a t_w}\frac{b_f}{2a}\left(1 - \frac{0{\cdot}024 t_f}{a}\right)\right] \tag{26}$$

according to Ref. 4.

For joints with thin webs, a procedure for determining the ultimate moments similar to the tension field method for the shear capacity of beams with thin webs is proposed by Scheer *et al.*[1] The limit moment is determined as the sum of the critical moment and the moment due to tension field action.

In the following the results of the five methods described above will be compared with the experimental results on joints with thin webs reported in Ref. 1. The comparison between the formulae for thick webs and the experimental results on thin webs has been made in order to find out whether the methods for thick webs apply qualitatively to thin ones.

Table 1 presents the main specimen data and the respective ultimate moments. For more information the reader is referred to Ref. 1. One test is excluded from the table since its results were largely influenced by extremely large imperfections, as reported in Ref. 1, so that it had to be repeated on another specimen. Figure 5 represents graphically the ratios between the experimental and the theoretical results. To determine the limit moments, eqns (24)–(26) had to be slightly modified to make allowance for the influence of the normal and shear forces N_r and Q_r respectively on the corner moment, since these formulae do not apply to

TABLE 1
Test Specimen Data

Number	*Specimen*	a (mm)	t_w (mm)	b_f (mm)	t_f (mm)	σ_{yw} (N mm^2)	σ_{yf} (N mm^2)	M_u^{exp} (kN m)
1	A-10-10-2	200	1·0	150	10·1	217	299	−6·7
2	A-07-10-1	200	1·1	150	7·3	211	279	−6·3
3	A-07-13-2	200	1·25	150	7·35	226	259	−7·1
4	A-07-15-1	200	1·5	150	7·2	206	259	−7·4
5	A-05-10-1	200	1·1	150	5·4	211	366	−4·7
6	A-05-10-2	200	1·0	150	5·1	220	359	−5·2
7	A-05-10-3	200	1·0	150	5·1	220	359	−5·1
8	B-07-10-1	300	1·0	150	7·35	217	259	−8·9
9	B-07-10-2	300	1·0	150	7·35	217	259	−9·4

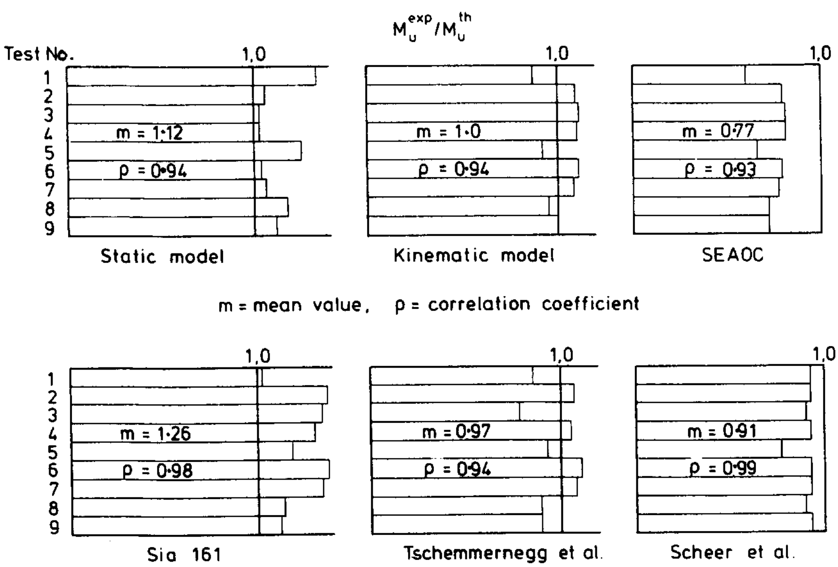

Fig. 5. Ratios M_u^{exp}/M_u^{th} for the different approaches.

the corner moment. The comparison shows that the predictions of all three methods for thin webs and the method of Tschemmernegg *et al.* are relatively close to the experimental results. As expected, eqn (24) predicts a far too large moment, whereas eqn (25) is far on the unsafe side. However, the results of all methods correlate well with the experimental results, suggesting that they might be used for design after a certain numerical manipulation. The design moment is equal to

$$M_d = M_u/\gamma_m \tag{27}$$

where the partial safety factor for the resistance may be determined according to the procedure described in Ref. 8. If this is applied to the formula of the 'kinematic' model, which is recommended here, a value of $\gamma_m = 1{\cdot}24$ is found.

Obviously the applicability of this formula is restricted to an experimentally verified range of geometric and loading parameters. An extrapolation of the formula to rectangular joints with dimensions $a \times b$ might be written as

$$M_u = -\frac{\sigma_{yw} t_w ab}{\sqrt{3}} \left(0{\cdot}65 + \frac{3{\cdot}45 t_f^2}{a t_w} \frac{\sigma_{yf}}{\sigma_y} \frac{b_f}{2b} \right) \tag{28}$$

but requires experimental verification.

DEFORMABILITY OF THE JOINT

If the joints are allowed to be stressed beyond the linear range, information must be provided for their deformation. Inclusion of the joint deformations is required for reasons of safety and is of major importance for the global behaviour of the overall frame. This applies especially in the case of sway frames subjected to lateral loads, where the additional deformations due to joint rotation may adversely affect the overall stability. In the following section two methods for the estimation of the joint limit rotation θ will be presented that correspond to the previously described models.

The kinematics of the failure mechanism on which the static model is based are shown in Fig. 6. Equating the external and internal works of the system yields

$$2M_p(\varphi + \theta) = M_u\theta + T_1 \frac{\sqrt{2}d_1}{4}(1 - \sin\theta - \cos\varphi) - T_2 \frac{\sqrt{2}a}{2} \sin\theta \tag{29}$$

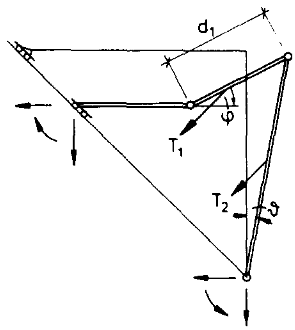

Fig. 6. The static model on the deformed state.

The kinematics of the model of Fig. 6 allow a quick, however gross, estimation of the rotation θ to be made. Indeed, the geometric compatibility of the failure mechanism requires that

$$\sin\varphi = \frac{d_1}{a}(\sin\theta + \cos\varphi - 1) \tag{30}$$

Let us assume that the failure mechanism proceeds by allowing the rotation θ to increase progressively, following a corresponding increase of the rotation φ. At some point, under the constraint imposed by the geometry of the mechanism, the rotation reaches its maximum value. Then for any further increase of φ, the rotation of θ begins to decrease (assuming that, except for the plastic hinges which allow for free rotation, the frame behaves elastically). We may consider that the maximum value of θ respresents the rotation at which the mechanism reaches its maximum capacity (since M_u becomes a minimum, requiring the least energy for the maximum value of θ; eqn (29)). Differentiation of eqn (30) with respect to φ suggests that θ reaches its maximum value when $\varphi = 45°$, with the corresponding maximum value of θ given by

$$\theta = \sin^{-1}\left[\frac{d_1}{a} + \frac{\sqrt{2}}{2}\left(1 - \frac{d_1}{a}\right)\right] - \frac{\pi}{4} \tag{31}$$

The values of θ calculated by eqn (31) compare well with the experimental values, as will be shown later, suggesting that eqn (31) gives a reasonable estimation of the rotations. A point that needs clarification here concerns the rotation φ. As may be revealed from the pictures of the joints tested experimentally,[1] the rotation φ is actually much smaller than 45°, being somewhere in the order of magnitude of θ. This is due to the fact that the frame does not elongate elastically, as assumed in this analysis, but yields along its top flange, elongating plastically to some extent and undergoing a smaller than 45° rotation φ. This explains why the static model appears to be relatively stiff, in terms of the calculated ultimate moment M_u, as compared with the results of the experiments. Indeed, calculating the ultimate moments M_u by means of eqn (29), based on the assumption that $\varphi = \theta$ and with θ given by eqn (31), one obtains values for M_u closer to the experimental results. Note that the maximum value of θ, as estimated by eqn (31), should not be affected significantly by the assumption that the angle φ is allowed to decrease, following a corresponding axial yield of the top flange.

From the kinematic model presented in Fig. 4, the rotation may be determined as the intersection between the M–θ curve, according to eqn (20) in connection with eqns (17)–(19), and the horizontal line through M_u, evaluated from eqn (22), as shown in Fig. 7. A comparison of these values of θ with those obtained experimentally suggests that the assumed failure mechanism of Fig. 4 is very close to the experimental one.

Once the pair (M_u–θ_u) has been determined (we recommend that eqn (22) should be used to determine M_u and eqn (31) to determine θ_u respectively, due to their relative simplicity, although the results when θ_u is determined by the kinematic model are much closer to the experimental ones) the complete moment–rotation behaviour can be approximated by a bilinear elastoplastic curve. A better approximation is achieved if a further point on the M–θ curve is determined. The experimental results indicate that the linear range extends beyond the critical buckling moment M_{cr}, which corresponds to shear stresses equal to the critical buckling stress of the panel zone τ_{cr}, under the assumption of simple supporting conditions. It is therefore possible to limit the linear range of the M–θ curve by the moment

$$M_{cr} = a^2 t_w \tau_{cr} \tag{32}$$

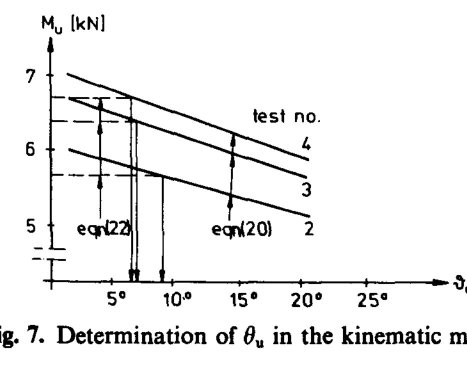

Fig. 7. Determination of θ_u in the kinematic model.

and the rotation by

$$\theta_{cr} = \tau_{cr}/G \tag{33}$$

The rotation θ_{cr} may approximately be set to 0 since its values for thin web panels are small, therefore implying that if the buckling moment is used as the design moment the joint could be numerically treated as stiff. The final curve can be completed by setting a parabola between the two points (M_u–θ_u) and (M_{cr}–0). In analytic terms the complete curve is expressed by the relations:

$$\theta = 0 \qquad \text{for } M \leqslant M_{cr} \tag{34a}$$

$$M = M_{cr} + (M_u - M_{cr})\sqrt{\frac{\theta}{\theta_u}} \qquad \text{for } M_{cr} < M < M_u \tag{34b}$$

$$M = M_u \qquad \text{for } M > M_u \tag{34c}$$

Figure 8 shows the results of some tests compared to the analytic curve given by eqns (34).

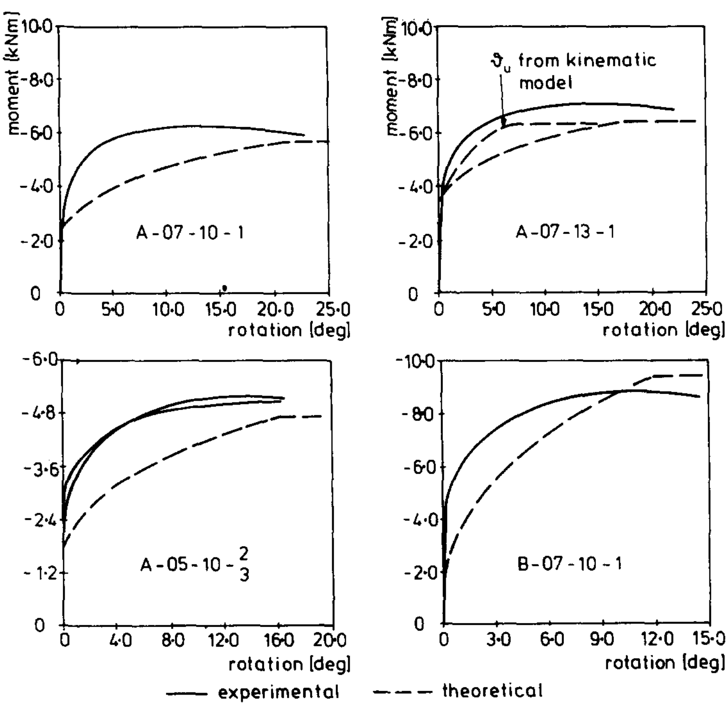

Fig. 8. Experimental vs theoretical M–θ curves.

CONCLUSION

Two different limit state models have been presented for the description of the carrying capacity of steel framed joints with slender web panels. Both models supply closed formulae for the determination of the ultimate limit moment of the joint. The theoretical results are in good agreement with corresponding experimental ones. Apart from the values of the moments, it is possible to predict the limit joint rotations that correspond to the above moments and to derive moment–rotation curves. These curves may be used as input data for the design of the overall frame. The curves agree well with the experimental ones. Application of the proposed models is restricted to the geometric conditions that have been examined experimentally.

REFERENCES

1. Scheer, J., Pasternak, H. & Schween, T., Zum Tragverhalten ausgesteifter Rahmenecken mit schlanken Stegen. *Der Stahlbau*, **60** (1991) 41–8.
2. Krawinkler, H. & Popov, E., Seismic behaviour of moment connections. *J. of the Struct. Div., ASCE*, **108** (ST 2) (1982) 373–91.
3. Bertero, V., Popov, E. & Krawinkler, H., Beam-column subassemblages under repeated loading. *J. of the Struct. Div., ASCE*, **98** (ST 5) (1972) 1137–59.
4. Tschemmernegg, F., *et al.*, Zur Nachgiebigkeit von Rahmenknoten. *Der Stahlbau*, **10** (1987) 299–306 and **58** (1989) 45–52.
5. Ermopoulos, J., & Vayas, I., Zum Tragverhalten von Rahmen mit verformbaren Knoten *Der Stahlbau*, **60** (1991) 326–32.
6. Recommended lateral force requirements and commentary. Structural Engineers Association of California, San Francisco, Calif., 1988.
7. Sia Norm 161: Stahlbauten, Draft 9.4.90, Schweizerischer Ingeniuer – und Architekten – Verein.
8. Eurocode 3 – Annex Z., Procedure for the determination of design resistances from tests Commission of the European Community, 1990.